A SOLUTION FOR NONLINEAR STABILITY ANALYSIS OF QFT CONTROLLERS DESIGNED FOR HYDRAULICALLY ACTUATED SYSTEMS

Masoumeh Esfandiari and Nariman Sepehri
Department of Mechanical Engineering, University of Manitoba, Winnipeg, Manitoba, Canada
E-mail: umesfand@cc.umanitoba.ca; nariman.sepehri@umanitoba.ca

Received March 2015, Accepted August 2015
No. 15-CSME-08, E.I.C. Accession 3783

ABSTRACT

Quantitative feedback theory (QFT) is a well-established technique to design robust and linear controllers. However, the important open problem of extending the small signal stability to nonlinear stability verification has remained an ongoing research in the design of QFT controllers. In this paper, we show that Takagi–Sugeno (T–S) fuzzy modeling approach and its stability theory provide a new opportunity to study the nonlinear stability of QFT controllers in fluid power systems. To validate the approach, two case studies are provided first. The first case study establishes the reliability of the approach by confirming the results for a hydraulic system of which nonlinear stability has already been proven. The second case study establishes that using the proposed approach, we can further study and extend the stability region of previously developed hydraulic controllers to include parametric uncertainty. Followed by the successful validation of the effectiveness of our approach through these two case studies, the stability of a QFT position controller, for which the nonlinear stability was never proven, is investigated.

Keywords: hydraulic actuators; quantitative feedback theory; stability analysis; linear matrix inequalities; Takagi–Sugeno fuzzy modeling.

UNE SOLUTION POUR L'ANALYSE DE LA STABILITÉ NON-LINÉAIRE DE CONTRÔLEURS QFT CONÇUS POUR DES SYSTÈMES ACTIONNÉ HYDRAULIQUEMENT

RÉSUMÉ

La technique de la théorie quantitative de la rétroaction (QFT) est une technique bien établie pour la conception de contrôleurs robustes linéaires. Cependant, l'important problème, encore non résolu, d'étendre la stabilité des faibles signaux à la vérification de la stabilité non-linéaire est toujours en cours de recherche pour la conception de contrôleurs QFT. Dans cet article, nous démontrons que l'approche Takagi–Sugeno (T–S) de modélisation d'ensembles flous, et sa théorie de stabilité procure une nouvelle occasion d'étudier la stabilité non-linéaire de contrôleurs QFT dans des systèmes à énergie à base de fluide. Pour valider cette approche, nous examinons deux cas. Le premier établit la fiabilité de l'approche en confirmant les résultats pour un système hydraulique dont la stabilité a déjà été prouvée. Le second cas établit qu'en utilisant l'approche proposée, nous pouvons pousser la recherche et étendre la région de la stabilité des contrôleurs déjà développée pour inclure une incertitude paramétrique. À la suite du succès de la validité de l'efficacité de notre approche à travers ces deux cas, la stabilité d'un contrôleur de position, pour lequel la stabilité non-linéaire n'a jamais été prouvée, est investiguée.

Mots-clés : contrôleurs actionnés hydrauliquement; théorie quantitative de rétroaction; analyse de stabilité; inégalités de matrice linéaire; modélisation d'ensembles flous Takagi–Sugeno.

1. INTRODUCTION

Hydraulic actuators have high force-to-weight ratio, linear movement and fast response [1]. These features make hydraulic actuators an excellent choice for a wide range of industrial applications such as crane operation [2], aerial work platforms [3, 4], automotive active suspension [5], and force/torque emulation of space manipulators [6]. Various control strategies have been proposed for position and force control of hydraulic actuators for the above applications. Adaptive [7], sliding mode [8], Lyapunov [9], and back-stepping [10] controllers are examples of successful nonlinear controllers. Linear controllers have also been designed to control hydraulic actuators such as PID [11], H_∞ [12], and quantitative feedback theory (QFT) controllers [13, 14].

Compared to nonlinear controllers, the popularity of linear controllers is due to their simple design and low computational burden [15]. Amongst the linear controller design techniques, quantitative feedback theory (QFT) is an excellent tool for designing controllers that are robust to parametric uncertainties and system faults. QFT design technique allows graphical representation of all design criteria including stability, reference tracking, disturbance rejection, control effort minimization, and noise attenuation, for the entire range of parametric uncertainties in a single Nichols Chart. As a result, a trade-off between controller complexity and fulfilling design criteria is achievable through loop shaping. QFT controllers are fixed-gain and linear, which only use the output feedback. As a result, these controllers require less hardware and easier implementation as compared with nonlinear and adaptive robust control schemes [9, 16]. Developing such robust and fault-tolerant controllers for hydraulic actuators, is attractive, since these actuators are subjected to parametric uncertainties and faults. As an example, consider position control of aircraft hydraulic actuators that must be tolerant against cross-port (internal) leakage that is hard to visually inspect. Design of a controller that maintains the desired performance in the presence of actuator internal leakage is critical [17]. Other successful applications of QFT to design controllers for safety critical applications can be found in references [18-20]. Despite successful demonstrations of applying QFT controllers on systems with parametric uncertainties and faults, the stability analysis of these control systems is presently limited. In the original QFT design approach, the stability of the resulting control system is valid only over particular sets of inputs-outputs and in a small-signal sense [21]. Consequently, a QFT control system is considered stable if the maximum change in the output happens as a result of a finite and small change in the input [22]. In other words, the stability cannot be guaranteed if the control system is exposed to scenarios not included in the acceptable design range.

Extensive effort has been devoted by Banos [22, 25–27] to establish a general framework for the nonlinear stability synthesis in the QFT design process. Barreiro and Banos [22] employed conic bounding to incorporate the Input/output (I/O) stability bounds in the process of QFT controller design for memoryless nonlinear plants. Other efforts to incorporate nonlinear stability bounds in the design process of QFT controllers include the work by Wang et al. [23] who employed the Circle criterion in the process of QFT design to study the effects of time-varying gain on both the stability and performance of the control system. Oldak et al. [24] suggested using the describing function theory and the Circle criterion along with QFT design to avoid limit cycles. Absolute stability techniques like Circle criterion and Popov criterion put very conservative frequency-domain conditions on the design of QFT controllers [25]. Banos et al. [26] employed harmonic balance and multiplier theory. Harmonic balance provides an approximated solution to the global stability problem, but with relaxed conditions. Multiplier theory is a less conservative version of absolute stability; however, finding appropriate multipliers is qualitative [26]. In another work by Banos and Horowitz [27], Schauder fixed point theorem was used to achieve a special type of BIBO stability, called nonlinear quantitative stability. All of the above approaches are complex, in terms of adding extra computations and conditions during the design process and present either approximate stability results or a conservative design. Rigorous stability analysis can also be obtained using Lyapunov direct method, but the

challenge is to find a suitable Lyapunov function.

In this paper, we employ the Takagi–Sugeno (T–S) fuzzy modeling and the corresponding stability theory [28,29] to address the nonlinear stability problem of QFT controllers applied to hydraulically actuated control systems. Towards this goal, the hydraulic system with its parametric uncertainties is represented as a T–S fuzzy model, which is a weighted sum of local linear models. T–S fuzzy models for hydraulic actuators have been previously used in the process of designing fuzzy static output feedback controllers based on parallel distributed compensation scheme [30,31]. In our paper, however, the T–S fuzzy model of the hydraulic actuator is, for the first time, blended with an already designed QFT controller to explore the nonlinear stability of its closed-loop system. Stability conditions of the closed-loop system are presented in the form of linear matrix inequalities (LMIs), which can be solved by available LMI Toolboxes [32,33]. Using the above procedure, and without assigning conservative conditions on QFT controllers, a solution for the nonlinear stability analysis of QFT controllers is provided. In fact, the nonlinear stability analysis becomes independent from the design process of QFT controllers. Several examples are included to support the theoretical developments. At the end, the paper establishes that the T–S fuzzy model derived for hydraulic actuators with the corresponding analysis approach, produces correct stability results, can be used to extend stability regions for some existing controllers and, is reliable to consider when studying the nonlinear stability of QFT controllers in fluid power systems.

The remaining of this paper is organized as follows. In Section 2, a T–S fuzzy model describing the nonlinear functions of a valve-controlled single-rod hydraulic actuator is derived. In Section 3, the functionality of T–S fuzzy models and the corresponding stability theory is first verified by considering two case studies. The first case study is a robust nonlinear controller previously designed based on the passivity theory for the pressure control of a hydraulic actuator [16]. The stability of this system is re-confirmed using the T–S fuzzy modeling approach. The second case study relates to a bilateral haptic control system of a hydraulic actuator, which was previously designed based on Lyapunov stability theory [34]. Here, the proposed approach is used to not only re-confirm the stability results, but also extend the stability region to include parametric uncertainties. Having the validity of the approach established, in Section 3.3 the nonlinear stability of a QFT position controller [14] for an electro-hydraulic actuator with parametric uncertainties is investigated for the first time. Conclusions are presented in Section 4.

2. T–S FUZZY MODEL OF A VALVE-CONTROLLED SINGLE-ROD HYDRAULIC ACTUATOR

2.1. Nonlinear Model

Schematic of a valve-controlled single-rod hydraulic actuator in contact with a spring dominant environment is shown in Fig. 1. In the hydraulic actuator, the control signal causes the valve spool to move. The following dynamic equation shows the relationship between the spool displacement (x_v) and the control signal (u_v):

$$\ddot{x}_v = -\omega_v^2 x_v - 2\xi_v \omega_v v_v + k_{sp}\omega_v^2 u_v \tag{1}$$

where ω_v is the undamped natural frequency of the valve; ξ_v is the valve damping ratio and k_{sp} is the valve spool position gain. By spool displacement, the valve controls the flow of the hydraulic fluid into and out of the chambers, given by Q_1 and Q_2:

$$Q_1 = K_v w x_v \sqrt{\frac{P_s - P_r}{2} + \mathrm{sgn}(x_v)\left(\frac{P_s + P_r}{2} - P_1\right)} \tag{2a}$$

$$Q_2 = K_v w x_v \sqrt{\frac{P_s - P_r}{2} + \mathrm{sgn}(x_v)\left(P_2 - \frac{P_s + P_r}{2}\right)} \tag{2b}$$

$$\mathrm{sgn}(x_v) = \begin{cases} 1 & x_v \geq 0 \\ -1 & x_v < 0 \end{cases} \tag{2c}$$

In Eqs. (2), P_s and P_r are the hydraulic supply and return pressures, respectively. P_1 and P_2 denote the pressures in chambers 1 and 2, respectively. The orifice area gradient of the servovalve is shown as w and constant $K_v = \sqrt{2/\rho} C_d$is the flow coefficient where C_d is the servovalve orifice coefficient of discharge and ρ is the density of the hydraulic fluid.

The input and output flows in turn change the pressure in each chamber of the actuator as follows:

$$\dot{P}_1 = \frac{\beta}{V_1}(Q_1 - A_1 v_p) \tag{3a}$$

$$\dot{P}_2 = \frac{\beta}{V_2}(-Q_2 + A_2 v_p) \tag{3b}$$

In Eqs. (3), A_1 and A_2 refer to the effective piston areas in each side of the actuator and β is the effective bulk modulus of the hydraulic fluid. The volume of the hydraulic fluid in each side of the actuator is given by variables V_1 and V_2 as follows:

$$V_1 = V_{01} + A_1 x_p \tag{4a}$$

$$V_2 = V_{02} - A_2 x_p \tag{4b}$$

where x_p is the actuator displacement, and V_{01} and V_{02} are the initial fluid volume in each side of the actuator, respectively. The differential pressure between chambers 1 and 2 generates the actuator force f_a as follows:

$$f_a = A_1 P_1 - A_2 P_2 = A_1(P_1 - \alpha P_2) = A_1 P_L \tag{5}$$

where P_L is defined as the output pressure. The ratio between piston areas in each side of the actuator is shown by α=A_2/A_1 which has the following relationship with the flows [35–37]:

$$\alpha = \frac{A_2}{A_1} = \frac{Q_2}{Q_1} \tag{6}$$

The actuator force f_a is applied to the environment according to the following dynamic equation:

$$\ddot{x}_p = \frac{1}{m}(f_a - k x_p - d v_p - f_d) \tag{7}$$

In the above equation, the combined mass of the piston and the environment is denoted by m and lumped at the end of the rod (see Fig. 1). Parameter d shows the combined environment damping and the actuator viscous damping. The stiffness of the environment is shown by k, and f_d represents disturbance forces including dry friction between piston and the cylinder walls. In order to control the actuator force f_a, the output pressure P_L should be controlled. To derive a differential equation for P_L, first Eqs. (2) are substituted into Eq. (6), which results in the following equation:

$$P_s = \varepsilon(\alpha^2 P_1 + P_2) \tag{8a}$$

$$\varepsilon = \begin{cases} \frac{1}{\alpha^2} & x_v \geq 0 \\ 1 & x_v < 0 \end{cases} \tag{8b}$$

The above equation describes the relationship between the actuator pressures P_1 and P_2, and the supply pressure P_s. Next, using the definition of $P_L = P_1 - \alpha P_2$, Eqs. (3) and (8), and assuming $P_r = 0$, the following differential equation for P_L is obtained:

$$\dot{P}_L = \beta \left(\frac{1}{V_{01} + A_1 x_p} + \frac{\alpha^2}{V_{02} - A_2 x_p} \right) (Q_1 - A_1 v_p) \tag{9}$$

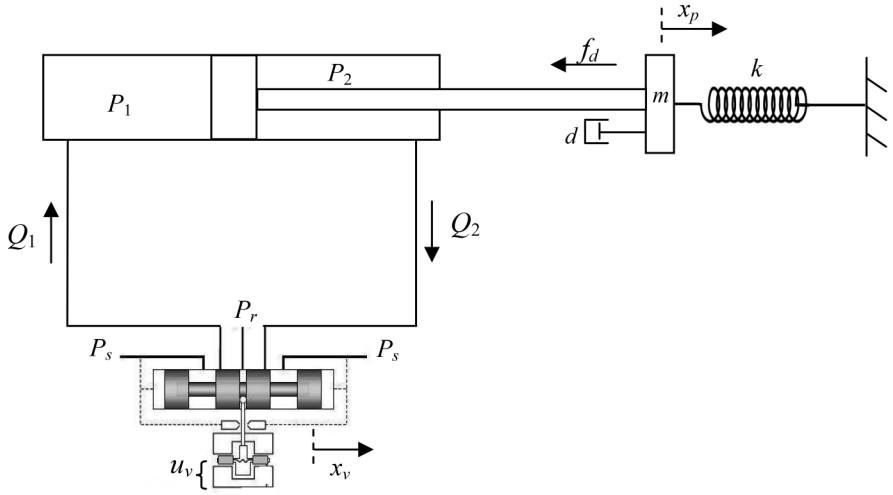

Fig. 1. Schematic of a valve-controlled single-rod hydraulic actuator.

Combining Eqs. (2) and (8), Q_1 is written as a function of P_L and x_v as follows:

$$Q_1 = \frac{K_v w x_v}{\sqrt{1+\alpha^3}} \sqrt{(1+\alpha)\frac{P_s}{2} + \mathrm{sgn}(x_v)\left[(1-\alpha)\frac{P_s}{2} - P_L\right]} \tag{10}$$

Now, the entire nonlinear model of the single-rod hydraulic actuator is written based on (1)–(10):

$$\dot{x}_p = v_p \tag{11a}$$

$$\dot{v}_p = \frac{A_1}{m}\left(P_L - \frac{k}{A_1}x_p - \frac{d}{A_1}v_p - \frac{f_d}{A_1}\right) \tag{11b}$$

$$\dot{P}_L = \beta\left(\frac{1}{V_{01}+A_1 x_p} + \frac{\alpha^2}{V_{02}-A_2 x_p}\right)\left(\frac{K_v w x_v}{\sqrt{1+\alpha^3}}\sqrt{(1+\alpha)\frac{P_s}{2} + \mathrm{sgn}(x_v)\left[(1-\alpha)\frac{P_s}{2} - P_L\right]} - A_1 v_p\right) \tag{11c}$$

$$\dot{x}_v = v_v \tag{11d}$$

$$\dot{v}_v = -\omega_v^2 x_v - 2\xi_v \omega_v v_v + k_{sp}\omega_v^2 u_v \tag{11e}$$

The nonlinear model (11) is used in the next section, to establish a T–S fuzzy model for the single-rod hydraulic actuator.

2.2. T–S Fuzzy Model

In order to obtain a T–S fuzzy model for the system described by (11), the sector nonlinearity approach is employed [29]. This approach guarantees an exact T–S fuzzy representation for the original nonlinear model [29]. During the construction of T–S fuzzy model by sector nonlinearity approach, no parts of the original nonlinear system is removed or approximated. In fact using the sector nonlinearity approach, the derived T–S fuzzy model is only a different mathematical representation of the original nonlinear system within a sector. In this method, each nonlinear term in Eqs. (11) is represented in a sector, i.e. $z(\vec{\mathbf{x}}(t))x_i(t) \in [a_1 \quad a_2]x_i(t)$, where $x_i(t)$ is one of the system variables in the state vector $\vec{\mathbf{x}} = [x_p \quad v_p \quad P_L \quad x_v \quad v_v]^{\mathrm{T}}$, and $z(\vec{\mathbf{x}}(t))x_i(t)$ represents any nonlinear terms in (11). In the sector $[a_1 \quad a_2]x_i(t)$, the term $z(\vec{\mathbf{x}}(t))x_i(t)$ is represented as $[M_1 a_1 + M_2 a_2]x_i(t)$ where M_1 and M_2 are positive nonlinear membership functions such that $\sum_{i=1}^{2} M_i = 1$

and $a_{i(i=1,2)}$ are the extremums of $z(\vec{\mathbf{x}}(t))$. In this section, by applying the above approach, the nonlinear dynamic eqsuations (11) will be represented as

$$\dot{\vec{\mathbf{x}}}(t) = \sum_{\rho=1}^{r} q_\rho(z(\vec{\mathbf{x}}(t)))\left(A_\rho \vec{\mathbf{x}}(t)\right)$$

which is a weighted sum of local linear models, $A_\rho \vec{\mathbf{x}}(t)$. The construction of matrices $\boldsymbol{A}_\rho$ and membership functions $q_\rho(z(\vec{\mathbf{x}}(t)))$ is described step-by-step below. The nonlinearity of (11) originates from the differential equation of the output pressure P_L, which is rewritten as follows:

$$\dot{P}_L = z_1(t)z_2(t)x_v - A_1 z_2(t)v_p \tag{12}$$

where $z_1(t)$ and $z_2(t)$ are

$$z_1(t) = \frac{K_v w}{\sqrt{1+\alpha^3}}\sqrt{(1+\alpha)\frac{P_s}{2} + \mathrm{sgn}(x_v)\left[(1-\alpha)\frac{P_s}{2} - P_L\right]} \tag{13a}$$

$$z_2(t) = \frac{\beta}{V_{01}+A_1 x_p} + \frac{\alpha^2\beta}{V_{02}-A_2 x_p} \tag{13b}$$

Here, we establish sectors and rewrite the nonlinear functions $z_1(t)$ and $z_2(t)$ in (13) as $z_1(t)x_v \in [g_2 \quad g_1]x_v$ and $z_2(t)\,v_p \in [h_2 \quad h_1]\,v_p$. First, consider the nonlinear function $z_1(t)$, which can be rewritten as follows:

$$z_1(t) = G_1(z_1(t))g_1 + G_2(z_1(t))g_2 \tag{14}$$

where $G_{i(i=1,2)}(z_1(t))$ are positive membership functions defined as follows:

$$G_1(z_1(t)) = \frac{z_1(t)-g_2}{g_1-g_2} \tag{15a}$$

$$G_2(z_1(t)) = \frac{g_1-z_1(t)}{g_1-g_2} \tag{15b}$$

and $\sum_{i=1}^{2} G_i(z_1(t)) = 1$. In the above equations, g_1 and g_2 are the extremums of $z_1(t)$:

$$g_1 = \max_{x_v(t),P_L(t)}(z_1(t)) \tag{16a}$$

$$g_2 = \min_{x_v(t),P_L(t)}(z_1(t)) \tag{16b}$$

To determine the extremums, we observe that $z_1(t)$ depends on the value of the state P_L, the sign of the state x_v, and the values of parameters K_v, w, α, and P_s. For now, consider that there is no uncertainty in the values of the system parameters. To find out the extremums of $z_1(t)$, the variation range for P_L is considered for $x_v \geq 0$, $[P_{L\min+} \; P_{L\max+}]$, and $x_v < 0$, $[P_{L\min-} \quad P_{L\max-}]$. It can be easily observed that as P_L increases, $z_1(t)$ decreases for and increases for . Therefore, depending on the application, the extremums are found based on the following values:

$x_v \geq 0$:

$$z_1(t) = \frac{K_v w\sqrt{P_s - P_{L\min+}}}{\sqrt{1+\alpha^3}} \tag{17a}$$

$$z_1(t) = \frac{K_v w \sqrt{P_s - P_{L\max+}}}{\sqrt{1+\alpha^3}} \tag{17b}$$

$x_v < 0$:

$$z_1(t) = \frac{K_v w \sqrt{\alpha P_s + P_{L\min-}}}{\sqrt{1+\alpha^3}} \tag{17c}$$

$$z_1(t) = \frac{K_v w \sqrt{\alpha P_s + P_{L\max-}}}{\sqrt{1+\alpha^3}} \tag{17d}$$

Note that if the values of the parameters K_v, w, α, and P_s vary within sectors, they should also be considered in the calculation of the extremums of $z_1(t)$ in Eqs. (17).

The same procedure can be carried out for the nonlinear function $z_2(t)$:

$$z_2(t) = H_1(z_2(t))h_1 + H_2(z_2(t))h_2 \tag{18}$$

The membership functions are defined as follows:

$$H_1(z_2(t)) = \frac{z_2(t) - h_2}{h_1 - h_2} \tag{19a}$$

$$H_2(z_2(t)) = \frac{h_1 - z_2(t)}{h_1 - h_2} \tag{19b}$$

where $\sum_{j=1}^{2} H_j(z_2(t)) = 1$, and h_1 and h_2 are the extremums of $z_2(t)$ and defined as follows:

$$h_1 = \max_{x_p(t)}(z_2(t)) \tag{20a}$$

$$h_2 = \min_{x_p(t)}(z_2(t)) \tag{20b}$$

To find the extremums h_1 and h_2, the solutions of the following equation should be calculated:

$$\frac{dz_2(t)}{dx_p} = \frac{A_1}{(V_{01} + A_1 x_p)^2} + \frac{\alpha^2 A_2}{(V_{02} - A_2 x_p)^2} = 0 \Rightarrow \tag{21a}$$

$$x_p = \frac{V_{02} - \sqrt{\alpha^3} V_{01}}{A_2 + \sqrt{\alpha^3} A_1} \;\Rightarrow\; z_2(t) = \frac{\beta A_1(\sqrt{\alpha^3} + \alpha^2) + \beta A_2 \left(1 + \frac{\alpha^2}{\sqrt{\alpha^3}}\right)}{V_{01}A_2 + V_{02}A_1} \tag{21b}$$

$$x_p = \frac{V_{02} + \sqrt{\alpha^3} V_{01}}{A_2 - \sqrt{\alpha^3} A_1} \;\Rightarrow\; z_2(t) = \frac{\beta A_1(-\sqrt{\alpha^3} + \alpha^2) + \beta A_2 \left(1 - \frac{\alpha^2}{\sqrt{\alpha^3}}\right)}{V_{01}A_2 + V_{02}A_1} \tag{21c}$$

In addition to the solution (21), the value of $z_2(t)$ should be calculated in boundaries of x_p, which are 0 and L (cylinder stroke) as follows:

$$x_p = 0 \;\Rightarrow\; z_2(t) = \frac{\beta}{V_{01}} + \frac{\alpha^2 \beta}{V_{02}} \tag{22a}$$

$$x_p = L \;\Rightarrow\; z_2(t) = \frac{\beta}{V_{01} + A_1 L} + \frac{\alpha^2 \beta}{V_{02} - A_2 L} \tag{22b}$$

Now, based on solutions (21) and (22), the extremums of $z_2(t)$, forming the sector $[h_2 h_1]$ are determined. In the above solutions, the values of parameters β, V_{01}, V_{02}, A_1, A_2, α, and L were considered known

and constant. If they are considered uncertain, their ranges should be considered in the calculation of the extremums. Now using formulations (14) and (18) for $z_1(t)$ and $z_2(t)$ respectively, Eq. (12) is rewritten as follows:

$$\begin{aligned}\dot{P}_L &= (G_1(z_1(t))g_1 + G_2(z_1(t))g_2)(H_1(z_2(t))h_1 + H_2(z_2(t))h_2)x_v - A_1(H_1(z_2(t))h_1 + H_2(z_2(t))h_2)v_p \\ &= \left(\sum_{i=1}^{2} G_i(z_1(t))g_i\right)\left(\sum_{j=1}^{2} H_j(z_2(t))h_j\right)x_v - A_1\left(\sum_{j=1}^{2} H_j(z_2(t))h_j\right)v_p \end{aligned} \tag{23}$$

Since

$$\sum_{i=1}^{2} G_i(z_1(t)) = 1 \quad \text{and} \quad \sum_{j=1}^{2} H_j(z_2(t)) = 1$$

these membership functions can be easily factored as follows:

$$\dot{P}_L = \sum_{i=1}^{2}\sum_{j=1}^{2} G_i(z_1(t))H_j(z_2(t))(g_i h_j x_v - A_1 h_j v_p) \tag{24}$$

Since

$$\sum_{i=1}^{2}\sum_{j=1}^{2} G_i(z_1(t))H_j(z_2(t)) = 1$$

Eq. (24) can be combined with the rest of the linear equations in (11) to present the entire hydraulic actuator equations as follows:

$$\dot{\vec{\mathbf{x}}}(t) = \sum_{i=1}^{2}\sum_{j=1}^{2}(G_i(z_1(t))H_j(z_2(t)))(\mathbf{A}_{ij}\vec{\mathbf{x}}(t) + \mathbf{B}u_v) \tag{25}$$

where $\vec{\mathbf{x}} = [x_p \quad v_p \quad P_L \quad x_v \quad v_v]^T$, and $\mathbf{A}_{ij}$ and $\mathbf{B}$ are given as follows:

$$\mathbf{A}_{ij} = \begin{bmatrix} 0 & 1 & 0 & 0 & 0 \\ \frac{-k}{m} & \frac{-d}{m} & \frac{A_1}{m} & 0 & 0 \\ 0 & -A_1 h_j & 0 & h_j g_i & 0 \\ 0 & 0 & 0 & 0 & 1 \\ 0 & 0 & 0 & -\omega_v^2 & -2\zeta_v\omega_v \end{bmatrix} \tag{26a}$$

$$\mathbf{B} = [0 \quad 0 \quad 0 \quad 0 \quad k_{sp}\omega_v^2]^T \tag{26b}$$

Equation (25) represents the nonlinear model (11) as weighted sum ($\sum_{i=1}^{2}\sum_{j=1}^{2} G_i H_j$) of local linear models $\mathbf{A}_{ij}\vec{\mathbf{x}}(t) + \mathbf{B}u_v$.

In the derivation of Eq. (25), parametric uncertainties were not considered. If the original nonlinear system in (11) is subjected to any bounded parametric uncertainties, they should be equivalently incorporated in the T–S fuzzy model. To include uncertainty related to a system parameter into the T–S fuzzy model a representation analogous to Eqs. (14) or (18) can be considered [30]. For example, if the environmental stiffness is an unknown value in sector $[k_2 = k_{\min} k_1 = k_{\max}]$, it can be rewritten as:

$$k = S_1(k)k_1 + S_2(k)k_2 \tag{27}$$

where $S_1(k)$ and $S_2(k)$ are membership functions defined as:

$$S_1(k) = \frac{k - k_2}{k_1 - k_2} \tag{28a}$$

$$S_2(k) = \frac{k_1 - k}{k_1 - k_2} \tag{28b}$$

The nonlinear model of the single-rod hydraulic actuator in Eqs. (11) with the added parametric uncertainty in the stiffness of the environment is now represented as follows:

$$\dot{\vec{\mathbf{x}}}(t) = \sum_{i=1}^{2}\sum_{j=1}^{2}\sum_{l=1}^{2} G_i(z_1(t)H_j(z_2(t))S_l(k)(\mathbf{A}_{ijl}\vec{\mathbf{x}}(t) + \mathbf{B}u_v) \tag{29a}$$

$$A_{ijl} = \begin{bmatrix} 0 & 1 & 0 & 0 & 0 \\ \frac{-k_l}{m} & \frac{-d}{m} & \frac{A_1}{m} & 0 & 0 \\ 0 & -A_1 h_j & 0 & h_j g_i & 0 \\ 0 & 0 & 0 & 0 & 1 \\ 0 & 0 & 0 & -\omega_v^2 & -2\zeta_v\omega_v \end{bmatrix} \tag{29b}$$

Other uncertain parameters can also be included using a similar manner as in for the stiffness case in Eqs. (27) and (28). The summations in Eqs. (29) can then be aggregated as one summation similar to the general formulation outlined by [29]:

$$\dot{\vec{\mathbf{x}}}(t) = \sum_{\rho=1}^{8} q_\rho(z(t))(\mathbf{A}_\rho^*\vec{\mathbf{x}}(t) + \mathbf{B}_\rho^* u_v) \tag{30}$$

where $\rho = l + 2(j-1) + 4(i-1)$, $\mathbf{A}_\rho^* = \mathbf{A}_{ijl}$, $\mathbf{B}_\rho^* = \mathbf{B}$ and $q_\rho = G_i(z_1(t))H_j(z_2(t))S_l(k)$.

The single-rod hydraulic actuator equations in (11) are then mapped onto (30) as follows:

Model rule 1:
IF z_1(t) is G_1, and z_2(t) is H_1, and k is S_1
THEN $\dot{\vec{\mathbf{x}}}(t) = \vec{A}_1^*\vec{\mathbf{x}}(t) + \vec{B}_1^* u_v$
⋮
Model rule 8:
IF z_1(t) is G_2, and z_2(t) is H_2, and k is S_2
THEN $\dot{\vec{\mathbf{x}}}(t) = \vec{A}_8^*\vec{\mathbf{x}}(t) + \vec{B}_8^* u_v$

The T–S fuzzy model of hydraulic actuator described by Eq. (30) can be used for double-rod hydraulic actuators when α=1, and in free motion when k=0. Furthermore, for hydraulic actuators in closed-loop control systems, the above T–S fuzzy model must be augmented by the controller dynamics. For a QFT controller, then the equations describing it, can be added to the above T–S fuzzy model, (will be discussed in Section 3.3). Accordingly, the final closed-loop system can be presented as follows:

$$\dot{\vec{\mathbf{x}}}(t) = \sum_{\rho=1}^{r} (q_\rho(z(t)))(\mathbf{A}_\rho^{cl}\vec{\mathbf{x}}(t)) \tag{31}$$

where $\vec{\mathbf{x}}(t)$ represents the state vector of the closed-loop system, and $\mathbf{A}_\rho^{cl}$ represents the local linear models. Total number of fuzzy rules is shown by r.

Table 1. Values of parameters used in Eqs. (33).

Parameter	Nominal value
Supply pressure, P_s (MPa)	10.3
Hydraulic coefficient, α (N/m^3)	1.51×10^{10}
Hydraulic coefficient, β (1/sec)	1.0
Hydraulic coefficient, γ (kg$^{0.5}$/m$^{1.5}$sec^2)	7.28×10^8
Load spring stiffness, k (kN/m)	16
Mass, m (kg)	24
Viscous damping, b (N·sec/m)	310
Piston area, A (m^2)	3.26×10^4

2.3. Stability of T–S Fuzzy Systems

Consider the T–S fuzzy model of a closed-loop system, described by Eq. (31). The equilibrium point of this system is globally asymptotically stable if there exists a common positive definite matrix $\boldsymbol{P}$ such that for $\rho = 1, \ldots, r$ [28, 29]:

$$\begin{cases} \mathbf{P} = \mathbf{P}^T > 0 \\ \mathbf{A}_\rho^{clT}\mathbf{P} + \mathbf{P}A_\rho^{cl} < 0 \end{cases} \tag{32}$$

Conditions (32) can be stated as linear matrix inequalities (LMIs) [29, 32]. When LMIs become feasible, it means that the solution matrix $\mathbf{P}$ is found [32, 33]. Any stability results for the system in Eq. (31) can then be extended for the original nonlinear model due to the zero modeling error between the original nonlinear model and the established T–S fuzzy model [29].

3. CASE STUDIES

In this section, the approach for stability analysis using T–S fuzzy model of hydraulic actuation systems are employed to analyze the stability of three systems. The first case study relates to a nonlinear pressure controller, designed for a hydraulic actuator [16]. The stability of this control system was proven previously using passivity theory. Here, the stability is verified again using the T–S fuzzy modeling and its stability analysis approach. This case study establishes that the modeling approach presented earlier is valid and can be used with confidence in cases for which stability analysis is limited or non-existent.

The second case study relates to a bilateral haptic control scheme for hydraulic actuators designed based on Lyapunov stability theory [34]. The stability of this control system was not studied in the presence of parametric uncertainties. We therefore extend the stability analysis of this control system to find the range of system parameters for which the closed-loop system remains stable.

Having established the validity of the proposed approach through two case studies, we prove the nonlinear stability of a QFT controller previously designed for the position control of a hydraulic actuator [14]. Unlike the first and the second case studies, the stability verification of this system, prior to this study, was limited in a small-signal sense. Here we employ T–S fuzzy modeling and corresponding stability analysis and, for the first time, prove the nonlinear stability of the QFT position controller for a parametrically uncertain hydraulic actuator.

3.1. Case Study 1: Nonlinear Force/Pressure Controller by Alleyne and Liu [16]

The purpose of this case study is to show that using T–S fuzzy modeling and corresponding stability analysis can indeed produce stability results similar to the ones obtained previously. Alleyne and Liu [16] developed a robust nonlinear force/pressure controller for a hydraulic actuator. In their experimental set-up, the cylinder is attached to a slide in contact with a linear spring. The following equations were used to describe the

system:

$$\dot{\xi}_1 = \xi_2 \tag{33a}$$

$$\dot{\xi}_2 = -\frac{k}{m}\xi_1 - \frac{b}{m}\xi_2 + \frac{A}{m}x_1 \tag{33b}$$

$$\dot{x}_1 = \underbrace{-\alpha\xi_2 - \beta x_1}_{f_1(\xi,x_1)} + \underbrace{\gamma(\sqrt{P_s - \mathrm{sgn}(x_2)x_1})}_{g_1(\xi,x_1)}x_2 \tag{33c}$$

$$\dot{x}_2 = \underbrace{-\frac{1}{\tau}x_2}_{f_2(\xi,x_1,x_2)} + \underbrace{\frac{k_{sp}}{\tau}}_{g_2(\xi,x_1,x_2)}u \tag{33d}$$

where ξ_1 and ξ_2 indicate the slide position and the velocity, respectively. x_1 denotes the cylinder pressure differential, x_2 is the valve spool position, and u is the control signal. The output to be controlled is the pressure differential x_1. Description and the values for the parameters in (33) are provided in Table 1. Nonlinear functions $f_1(\xi,x_1)$, $f_2(\xi,x_1,x_2)$, $g_1(\xi,x_1)$ and $g_2(\xi,x_1,x_2)$ are used in the controller design. Accordingly, to achieve a stable force/pressure tracking system, the following control law was proposed by Alleyne and Liu [16]:

$$u \equiv \frac{1}{g_2}(-f_2 + \dot{x}_{2\text{desired}} - k_2 e_2) \tag{34a}$$

$$x_{2\text{desired}} \equiv \frac{1}{g_1}(-f_1 + \dot{x}_{1\text{desired}} - k_1 e_1) \tag{34b}$$

where $x_{1\text{desired}}$ and $x_{2\text{desired}}$ are the desired differential pressure and the desired valve spool displacement respectively. Errors e_1=x_1-$x_{1\text{desired}}$ and e_2=x_2-$x_{2\text{desired}}$, scaled by controller gains k_1 and k_2 are used to determine the control signal u. To determine the controller gains k_1 and k_2, first the controller equations in (34) are substituted in the system equations (33), to construct the error dynamic equations as follows:

$$\dot{e}_1 = -k_1 e_1 + g_1 e_2 \tag{35a}$$

$$\dot{e}_2 = -k_2 e_2 \tag{35b}$$

Using the passivity theory, the global stability has been proven, previously, providing the controller gains to be selected as $k_1 = \max(|g_1|)$ and $k_2 = k_{sp}/\tau > 0$ [16].

We now study the stability of the system in (35) using the T–S fuzzy models and corresponding stability theorem described earlier. First (35) must be represented by a T–S fuzzy model. Selecting the controller gains as $k_1 = \max(|g_1|) = \gamma\sqrt{P_s - \mathrm{sgn}(x_2)x_1} = 2.3 \times 10^{12}$ and $k_2 = k_{sp}/\tau = 1000$, the error dynamic equations (35) are represented by the following T–S fuzzy model:

$$\begin{bmatrix} \dot{e}_1 \\ \dot{e}_2 \end{bmatrix} = \sum_{i=1,2} T_i \begin{bmatrix} -k_1 & t_i \\ 0 & -k_2 \end{bmatrix} \begin{bmatrix} e_1 \\ e_2 \end{bmatrix} \tag{36}$$

In (36), the membership functions $T_{i(i=1,2)}$ are defined as follows:

$$T_1 = \frac{\gamma\sqrt{P_s - \mathrm{sgn}(x_2)x_1}) - t_2}{t_1 - t_2} \tag{37a}$$

$$T_2 = \frac{t_1 - \gamma\sqrt{P_s - \mathrm{sgn}(x_2)x_1})}{t_1 - t_2} \tag{37b}$$

The extremums $t_{i(i=1,2)}$ are found for $P_L \in [-(2/3)P_s \quad (2/3)P_s] = [-7 \text{ MPa} \quad 7 \text{ MPa}]$. $(2/3)P_s$ is considered as the maximum output pressure as applied to hydraulic actuator [1]:

$$t_1 = \max(\gamma\sqrt{P_s - \text{sgn}(x_2)x_1}) = \gamma\sqrt{10.3 \text{ MPa} + 7 \text{ MPa}} = 3.4 \times 10^{12}\sqrt{\text{Pa}} \tag{38a}$$

$$t_2 = \min(\gamma\sqrt{P_s - \text{sgn}(x_2)x_1}) = \gamma\sqrt{10.3 \text{ MPa} - 7 \text{ MPa}} = 1.5 \times 10^{12}\sqrt{\text{Pa}} \tag{38b}$$

LMIs are now constructed based on conditions in (32), and two local linear models described by Eq. (36). Using Matlab LMI toolbox, the LMIs are found feasible given the following common positive definite matrix **P** as the solution:

$$P = \begin{bmatrix} 1.17 & -0.72 \\ -0.72 & 9.72 \times 10^8 \end{bmatrix} \tag{39}$$

Therefore, the closed-loop system is stable. This is exactly what was concluded based on the passivity theory used by Alleyne and Liu [16].

3.2. Case Study 2: Bilateral Haptic Controller by Zarei-nia and Sepehri [34]

Case study 1 showed that the T–S fuzzy models and corresponding stability can be reliably employed to investigate the nonlinear stability of hydraulic control systems. In this case study, we not only confirm the existing stability results, but also extend the results to include uncertainty in a system parameter used by the controller. Zarei-nia and Sepehri [34] developed a bilateral control system, which allows a hydraulic actuator to achieve a stable position tracking at the slave side while, at the master side, the haptic device provides the feeling of tele-presence to the operator. The following equations were used by them to present the dynamics of the whole system:

Slave side:

$$\dot{x}_1 = x_2 \tag{40a}$$

$$\dot{x}_2 = \frac{A}{m_s}x_3 - \frac{d}{m_s}x_2 - \frac{k_s}{m_s}x_1 \tag{40b}$$

$$\dot{x}_3 = \frac{-A}{C}x_2 + \frac{c_d w}{C\sqrt{\rho}}x_4\sqrt{P_s - \text{sgn}(x_4)x_3} \tag{40c}$$

$$\dot{x}_4 = \frac{-1}{\tau}x_4 + \frac{k_{sp}}{\tau}u \tag{40d}$$

Master side:

$$\dot{x}_5 = v_6$$

$$\dot{x}_6 = \frac{1}{m_m}(F_h + F_m - k_d x_6 - k_h x_5) \tag{40e}$$

At the slave side, x_1, x_2, x_3 and x_4 are the actuator position, velocity, differential pressure and valve spool displacement, respectively. The control input is the voltage to the servovalve of the hydraulic actuator, shown by u. At the master side, x_5 and x_6 are the haptic device displacement and the velocity, respectively. F_h is the input force, originated from the operator and F_m is the control input applied to the master. To implement a stable position tracking system, the following control laws were proposed by Zarei-nia and Sepehri [34]:

$$u = \left[-K_{p1}(x_1 - x_5) - K_{p2}x_3\right]\sqrt{P_s - \text{sgn}(x_4)x_3} \tag{41a}$$

$$F_m = K_{p3}(x_1 - x_5) + K_{p4}x_3 \tag{41b}$$

Table 2. Values of parameters in Eqs. (40).

Parameter	Nominal value
Supply pressure, P_s (MPa)	17.2
Hydraulic compliance, C (m^5/N)	2×10^{-13}
Spring stiffness, k_s (kN/m)	125
Piston and rod mass; slave side, m_s (kg)	12.3
Viscous damping coefficient, d (N·sec/m)	250
Piston area, A (m^2)	6.33×10^{-4}
Orifice coefficient of discharge, c_d	0.6
Hydraulic fluid density, ρ (kg/m^3)	847.15
time constant, τ (msec)	0.03
Valve orifice area gradient, w (m^2/m)	0.02075
Valve gain, k_{sp} (m/V)	2.79×10^{-5}
Inertia of master, haptic, m_m (kg)	0.545
Viscous coefficient at the master side, k_d (N·sec/m)	2
Stiffness of human arm, k_h (N/m)	1000

where K_{p1}, K_{p2}, K_{p3} and K_{p4} are constant gains. The description and values of the rest of the parameters are given in Table 2.

To construct the closed-loop dynamic equations, the controller equations (41) were substituted into the master and the slave equations (40). The equilibrium of the closed-loop system was determined by imposing $\dot{x}_{i(i=1\ldots6)} = 0$ as follows:

$$\vec{\mathbf{x}}_{eq} = \begin{bmatrix} x_{1eq} & x_{2eq} & x_{3eq} & x_{4eq} & x_{5eq} & x_{6eq} \end{bmatrix}^T = \begin{bmatrix} x_{1ss} & 0 & x_{3ss} & 0 & x_{5ss} & 0 \end{bmatrix}^T \tag{42}$$

where x_{1ss}, x_{2ss} and x_{3ss} were obtained as follows:

$$x_{1ss} = \frac{K_{p1}AF_h}{(K_{p2}K_{p3}k_s - K_{p1}K_{p4}k_s + K_{p1}k_hA + K_{p2}k_hk_s)} \tag{43a}$$

$$x_{2ss} = \frac{K_{p1}k_sF_h}{(K_{p2}K_{p3}k_s - K_{p1}K_{p4}k_s + K_{p1}k_hA + K_{p2}k_hk_s)} \tag{43b}$$

$$x_{3ss} = \frac{K_{p1}AF_h + K_{p2}k_sF_h}{(K_{p2}K_{p3}k_s - K_{p1}K_{p4}k_s + K_{p1}k_hA + K_{p2}k_hk_s)} \tag{43c}$$

Defining $\vec{e} = \vec{x} - \vec{x}_{eq}$, the following error states were derived:

$$\dot{e}_1 = e_2 \tag{44a}$$

$$\dot{e}_2 = \frac{A}{m_s}e_3 - \frac{d}{m_s}e_2 - \frac{k_s}{m_s}e_1 \tag{44b}$$

$$\dot{e}_3 = -\frac{A}{C}e_2 + \frac{c_dw}{C\sqrt{\rho}}e_4\sqrt{P_s - \mathrm{sgn}(e_4)(e_3 + x_{3ss})} \tag{44c}$$

$$\dot{e}_4 = -\frac{1}{\tau}e_4 + \frac{k_{sp}}{\tau}[-K_{p1}(e_1 - e_5) - K_{p2}e_3]\sqrt{P_s - \mathrm{sgn}(e_4)(e_3 + x_{3ss})} \tag{44d}$$

$$\dot{e}_5 = e_6 \tag{44e}$$

$$\dot{e}_6 = \frac{1}{m_m}(K_{p3}(e_1 - e_3) + K_{p4}e_3 - k_de_4 - k_he_5 \tag{44f}$$

In Eqs. (44), e_1, e_2, e_3 and e_4 are the actuator position error, velocity error, differential pressure error and valve spool displacement error, respectively. Error states e_5 and e_6 are the haptic device displacement error and the velocity error at the master side, respectively.

By employing Lyapunov stability theory, the authors have concluded the following conditions to guarantee the stability of the proposed controller for Eqs. (44):

$$\frac{9C}{7A} < \frac{K_{p2}}{K_{p1}} \tag{45a}$$

$$K_{p3} < \frac{k_h(K_{p2}A - K_{p1}C)}{7K_{p2}A - 5K_{p1}C} \tag{45b}$$

$$K_{p4} = K_{p3}\frac{C}{A} \tag{45c}$$

Now the stability analysis of (44) is re-examined using T–S fuzzy modeling and its stability approach. The only nonlinear term in (44) is represented as follows:

$$z(t) = \sqrt{P_s - \mathrm{sgn}(e_4)(e_3 + x_{3ss})} = \sum_{i=1}^{2} h_{si}H_{si}(z(t)) = \sum_{j=1}^{2} h_{cj}H_{cj}(z(t)) \tag{46}$$

This term appeared in both the system and the controller equations, respectively in (44c) and (44d). Therefore subscripts s and c are used to separately refer to this nonlinear term in Eqs. (44c) and (44d), respectively. Membership functions $H_{si(i=1,2)}$ and $H_{cj(j=1,2)}$ are defined as follows:

$$H_{c1}(z(t)) = \frac{z(t) - h_{c2}}{h_{c1} - h_{c2}} \tag{47a}$$

$$H_{c2}(z(t)) = \frac{h_{c1} - z(t)}{h_{c1} - h_{c2}} \tag{47b}$$

$$H_{s1}(z(t)) = \frac{z(t) - h_{s2}}{h_{s1} - h_{s2}} \tag{47c}$$

$$H_{s2}(z(t)) = \frac{h_{s1} - z(t)}{h_{s1} - h_{s2}} \tag{47d}$$

Using nominal value for the supply pressure given in Table 2, and for $P_L \in [-(2/3)P_s \quad (2/3)P_s] = [-11.5\text{ MPa} \quad 11.5\text{ MPa}]$, the extremums $h_{si(i=1,2)}$ and $h_{cj(j=1,2)}$ are found as follows:

$$\begin{aligned} h_{c1} &= h_{s1} = \max(z(t)) = \max(\sqrt{P_s - \mathrm{sgn}(e_4)(e_3 + x_{3ss})}) \\ &= \max(\sqrt{P_s - \mathrm{sgn}(x_4)(x_3)}) = \sqrt{17.2\text{ MPa} + 11\text{ MPa}} = 5310\sqrt{\text{Pa}} \end{aligned} \tag{48a}$$

$$\begin{aligned} h_{c2} &= h_{s2} = \in (z(t)) = \min(\sqrt{P_s - \mathrm{sgn}(e_4)(e_3 + x_{3ss})}) \\ &= \min(\sqrt{P_s - \mathrm{sgn}(x_4)(x_3)}) = \sqrt{17.2\text{ MPa} - 11.5\text{ MPa}} = 2490\sqrt{\text{Pa}} \end{aligned} \tag{48b}$$

Substituting Eq. (46) into Eqs. (44), results in the following equation:

$$\begin{bmatrix} \dot{e}_1 \\ \dot{e}_2 \\ \dot{e}_3 \\ \dot{e}_4 \\ \dot{e}_5 \\ \dot{e}_6 \end{bmatrix} = \sum_{i=1}^{2}\sum_{j=1}^{2} H_{si}(z(t))H_{cj}(z(t)) \begin{bmatrix} 0 & 1 & 0 & 0 & 0 & 0 \\ \frac{-k_s}{m_s} & \frac{-d}{m_s} & \frac{A}{m_s} & 0 & 0 & 0 \\ 0 & \frac{-A}{C} & 0 & \frac{c_d w}{C\sqrt{\rho}}h_{si} & 0 & 0 \\ \frac{-k_{sp}K_{p1}}{\tau} & 0 & \frac{-k_{sp}K_{p2}}{\tau}h_{cj} & \frac{-1}{\tau} & \frac{k_{sp}K_{p1}}{\tau} & 0 \\ 0 & 0 & 0 & 0 & 0 & 1 \\ \frac{K_{p3}}{m_m} & 0 & \frac{K_{p4}-K_{p3}}{m_m} & \frac{-k_d}{m_m} & \frac{k_h}{m_m} & 0 \end{bmatrix} \begin{bmatrix} e_1 \\ e_2 \\ e_3 \\ e_4 \\ e_5 \\ e_6 \end{bmatrix} \tag{49}$$

Eq. (49) accurately represents original nonlinear model (44). The T–S fuzzy stability analysis is now employed. First a set of controller gains that satisfies conditions (45) are substituted into (49); $K_{p1} = 0.05$, $K_{p2} = 2 \times 10^{-10}$, $K_{p3} = 0.0139$, and $K_{p4} = 4.4 \times 10^{-12}$. Next, linear matrix inequalities are constructed based on conditions (32), and the local linear models in Eq. (49).

By solving the LMIs using LMI toolbox, the common positive definite matrix **P** is found as follows:

$$P = \begin{bmatrix} 5.21 & 0.08 & 0.27 & 1.99 & 2.48 & -2.07 \\ 0.08 & 7.24 & -0.27 & -1.49 & 0.83 & 1.1 \\ 0.27 & -0.27 & 8.52 & 0.78 & 0.31 & -0.75 \\ 1.99 & -1.49 & 0.78 & 12.19 & 8.98 & 12.71 \\ 2.48 & 0.83 & 0.31 & 8.98 & 349 & 40.53 \\ -2.07 & 1.1 & -0.75 & 12.71 & 40.53 & 813 \end{bmatrix} \tag{50}$$

Therefore, the proof of the stability for the controller in Eq. (41) with conditions (45) has been confirmed for the values of the parameters given in Table 2. However, the controller equations (41) requires an exact value for the supply pressure P_s. The issue of uncertainty in the value of supply pressure was not discussed in the previous work by Zarei-nia and Sepehri [34]. Here, we further investigate the stability of the system in Eq. (49) having uncertainty in the supply pressure. To incorporate such uncertainty, extremums $h_{si(i=1,2)}$ are re-calculated considering variation of P_s from its nominal value (17.2 MPa), i.e., $P_s \in [13.8\text{ MPa} \quad 22.6\text{ MPa}]$. The values for the extremums are then determined to be $h_{s1} = 6137$ and $h_{s2} = 2144$. The positive definite matrix, $\boldsymbol{P}$, satisfying stability conditions (32), is determined to be

$$P = \begin{bmatrix} 11 & 0.3 & 1.5 & 3.3 & 3.8 & 0.8 \\ 0.3 & 11 & -0.4 & -1.9 & -1.2 & 2.1 \\ 1.5 & -0.4 & 14 & 1.3 & 0.4 & 0.1 \\ 3.3 & -1.9 & 1.3 & 18 & 14 & 18 \\ 3.8 & -1.2 & 0.4 & 14 & 622 & 72 \\ 0.8 & 2.1 & 0.1 & 18 & 72 & 1450 \end{bmatrix} \tag{51}$$

Selecting different gains for the controller based on conditions (45) may extend or limit the allowable uncertainty range for the supply pressure.

This case study shows that T–S fuzzy modeling and the corresponding stability theorem are not only effective to conclude the stability of a given control system, but also can be useful to extend the previously-developed stability results to include uncertainties.

3.3. Nonlinear Stability of QFT-based Positioning System, by Karpenko and Sepehri [14]

The previous two case studies established that the T–S fuzzy modeling approach is effective to investigate the stability of hydraulically actuated control systems. In this section, the approach is employed, for the first time, to study the nonlinear stability of QFT controllers. One important common feature between T–S fuzzy models and QFT controllers is linearity. A T–S fuzzy model is a combination of local linear models and QFT controllers are linear. Using this common feature, a systematic formulation for the nonlinear stability analysis of QFT-based hydraulic control systems, in the format of LMIs, is obtained. This process is now employed for nonlinear stability analysis of the QFT position controller developed earlier for a double-rod hydraulic actuator by Karpenko and Sepehri [14]. The equations describing the dynamics of the system to be controlled are shown below:

$$\dot{x}_p = v_p \tag{52a}$$

Table 3. Values of parameters in Eqs. (52).

Parameter	Nominal value	Uncertainty range
Effective piston area, A (mm^2)	633	–
Length of rod, L (mm)	610	–
Flow coefficient, K_v (mm$^{3/2}$/kg$^{3/2}$)	0.0292	–
Orifice area gradient, w (mm^2/mm)	13.2	–
Valve damping ratio, ξ_v	0.9	–
Valve natural frequency, ω_v (Hz)	150	–
Supply pressure, P_s (MPa)	17.2	13.8–18.6
Load mass, m (kg)	12.3	11–13.7
Total damping, d (N·sec/m)	250	200–300
Fluid bulk modulus, β (MPa)	689	345–1030
Spool position gain, k_{sp} (μm/V)	28	25–31
Load stiffness, k (kN/m)	30	0–60
Initial volume of chambers, V_{01} and V_{02} (cm^3)	234	–

$$\dot{v}_p = \frac{1}{m}(AP_1 - AP_2 - kx_p - dv_p) \tag{52b}$$

$$\dot{P}_1 = \frac{\beta}{V_1}\left(k_v w x_v \sqrt{\frac{P_s - P_r}{2} + \mathrm{sgn}(x_v)\left(\frac{P_s + P_r}{2} - P_1\right)} - Av_p\right) \tag{52c}$$

$$\dot{P}_2 = \frac{\beta}{V_2}\left(-k_v w x_v \sqrt{\frac{P_s - P_r}{2} + \mathrm{sgn}(x_v)\left(P_2 - \frac{P_s + P_r}{2}\right)} + Av_p\right) \tag{52d}$$

$$\dot{x}_v = v_v \tag{52e}$$

$$\dot{v}_v = -\omega_v^2 x_v - 2\xi_v \omega_v v_v + k_{sp}\omega_v^2 u_v \tag{52f}$$

Similar as in Section 2, x_p and v_p are the position and the velocity of the hydraulic actuator respectively. P_1 and P_2 denote pressures in chambers 1 and 2, respectively. x_v and v_v are the position and velocity of valve spool, respectively. The volume of hydraulic fluid in each side of the actuator is given by V_1 and V_2 (see Eqs. (4)). The system input is the voltage applied to the servovalve (u_v). Description and values for the rest of the parameters are given in Table 3.

Note that the system has uncertainties in the supply pressure (P_s), bulk modulus (β), effective mass (m), total damping (d), stiffness of the environment (k), and valve spool gain (k_{sp}). To provide an accurate position tracking for the hydraulic actuator despite the parametric uncertainties, QFT design technique was employed in [14]. Here a very brief description of the design process is provided; for more details readers are referred to [14]. The process starts by approximation of the nonlinear system in Eqs. (52) with a number of frequency response functions. Each of these frequency responses, is obtained by applying Fourier transformation on a particular pair of actuator position, x_p, from a desirable envelope of operation, shown by gray region in Fig. 2 and corresponding input voltage u_v, calculated by inverse dynamic model of (52), given in [14].

Then, using the derived frequency responses of the hydraulic actuator, the tracking and stability requirements for the closed-loop system are rendered in the Nichols chart in the format of QFT bounds. After that, a QFT controller is designed through a loop-shaping process where the frequency responses of the hydraulic actuator is manipulated by adding poles and zeros to the controller until the loop shape lies in the acceptable region in the Nichols chart. The acceptable region is defined as the outside of the closed stability bounds and above the open tracking bounds.

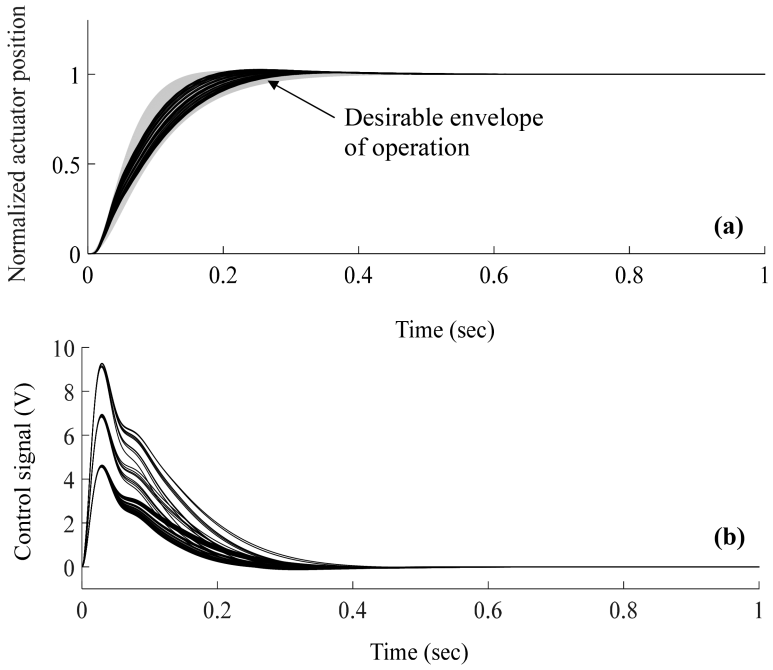

Fig. 2. Normalized actuator positions (solid lines) and the desirable envelope of operation (gray region); (b) corresponding control signals.

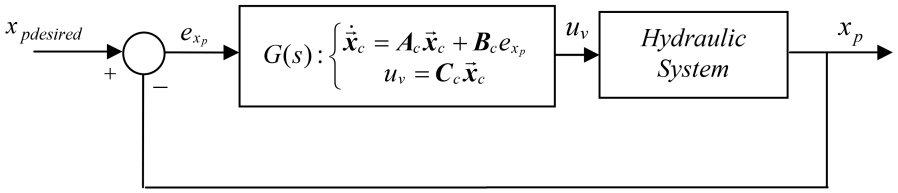

Fig. 3. Closed-loop system.

Using the above process, the following QFT controller was designed by Karpenko and Sepehri [14]:

$$G(s) = \frac{2.76 \times 10^6 (s+25)}{(s+16)(s^2+108s+120^2)} \tag{53}$$

Figure 2 shows the simulation results of applying QFT controller in Eq. (53) for the position tracking control of hydraulic actuator, given in Eqs. (52). Normalized actuator positions and corresponding control signals are shown for various combinations of the uncertain parameters given in Table 3 and different desired positions (0.02 m, 0.03 m, and 0.04 m). From Fig. 2, the output of the control system successfully converges to the desired position, while it remains within the desirable envelope of operation, shown by the gray region. The stable behaviour of the control system is also confirmed by experimental results in [14]. However, it has been argued that since the QFT controller is designed using a number of separate frequency responses, the closed-loop stability is guaranteed only if the plant is representable by one of these frequency responses [22, 26, 27]. Using T–S fuzzy modeling and its stability theorem, the stability of the closed-loop system is investigated directly for the nonlinear plant model in Eqs. (52). Therefore, the results will not be limited to the frequency responses which QFT controller was initially designed for.

Figure 3 shows the closed-loop structure of the system using the state-space representation of the controller (53) as follows:

$$\dot{\vec{\mathbf{x}}}_c = A_c\vec{\mathbf{x}}_c + B_c(x_{p\,\text{desired}} - x_p) \tag{54a}$$

$$u_v = C_c\mathbf{x}_c \tag{54b}$$

where $\vec{\mathbf{x}}_c = \begin{bmatrix} x_{c1} & \cdots & x_{c\lambda} \end{bmatrix}^T$ is the state vector of the controller and $\boldsymbol{A}_c$, $\boldsymbol{B}_c$, $\boldsymbol{C}_c$ are given as follows:

$$A_c = \begin{bmatrix} -124 & -16128 & -230400 \\ 1 & 0 & 0 \\ 0 & 1 & 0 \end{bmatrix} \tag{55a}$$

$$B_c = \begin{bmatrix} 1 & 0 & 0 \end{bmatrix}^T \tag{55b}$$

$$C_c = \begin{bmatrix} 0 & 2760000 & 690000000 \end{bmatrix} \tag{55c}$$

Note that in the closed-loop structure, the input to the controller is the error between the desired position and the actual position, $e_{x_p} = (x_{p\,\text{desired}} - x_p)$ and the output of the controller is the voltage signal u_v, applied to the servovalve (see Fig. 3).

With reference to Fig. 3, the control system contains the hydraulic actuator and the QFT controller. The T–S fuzzy model describing the double-rod hydraulic actuator given in Eqs. (52) can accurately be derived from the T–S fuzzy model of the single-rod hydraulic actuator in Eq. (25) for $\alpha = 1$, $A_1 = A_2 = A$, and $P_L = P_1 - P_2$:

$$\dot{\vec{\mathbf{x}}}(t) = \sum_{i=1}^{2}\sum_{j=1}^{2}\left(G_i\left(z_1(t)\right)H_j\left(z_2(t)\right)\right)\left(A_{ij}\vec{\mathbf{x}}(t) + Bu_v\right) \tag{56}$$

where $\vec{\mathbf{x}} = \begin{bmatrix} x_p & v_p & P_L & x_v & v_v \end{bmatrix}^{\mathrm{T}}$ is the vector of hydraulic states; $z_1(t)$ and $z_2(t)$ are terms previously explained in Section 2. $\boldsymbol{A}_{ij}$ and $\boldsymbol{B}$ are given as follows:

$$A_{ij} = \begin{bmatrix} 0 & 1 & 0 & 0 & 0 \\ \frac{-k}{m} & \frac{-d}{m} & \frac{A}{m} & 0 & 0 \\ 0 & -Ah_j & 0 & h_jg_i & 0 \\ 0 & 0 & 0 & 0 & 1 \\ 0 & 0 & 0 & -\omega_v^2 & -2\xi_v\omega_v \end{bmatrix} \tag{57a}$$

$$B = \begin{bmatrix} 0 & 0 & 0 & 0 & k_{sp}\omega_v^2 \end{bmatrix}^T \tag{57b}$$

Using the procedure discussed in Section 2, we further incorporate uncertainties in the supply pressure (P_s), bulk modulus (β), effective mass (m), total damping (d), stiffness of the environment (k), and valve spool gain (k_{sp}). This way, the same parametric uncertainties in the original nonlinear system (52) are incorporated in the corresponding T–S fuzzy model. The T–S fuzzy model of the double-rod hydraulic actuator, described by Eqs. (52) in the presence of parametric uncertainties, is as follows:

$$\dot{\vec{\mathbf{x}}}(t) = \sum_{i=1}^{2}\sum_{j=1}^{2}\sum_{l=1}^{2}\sum_{n=1}^{2}\sum_{r=1}^{2}\sum_{w=1}^{2} G_i(z_1(t))H_j(z_2(t))S_l(k)N_n(d)M_r(m)W_w(k_{sp})\left(A_{ijlnrw}\vec{\mathbf{x}}(t) + B_{ijlnrw}u_v\right) \tag{58}$$

The summations in (58) can be aggregated as follows:

$$\dot{\vec{\mathbf{x}}}(t) = \sum_{\rho=1}^{64}\left(q_\rho\left(z(t)\right)\right)\left(\mathbf{A}_\rho^*\vec{\mathbf{x}}(t) + \mathbf{B}_\rho^* u_v\right) \tag{59}$$

where $q_\rho(z(t))$, $\mathbf{A}^*_\rho$, and $\mathbf{B}^*_\rho$ are as follows:

$$q_\rho(z(t)) = G_i(z_1(t))H_j(z_2(t))S_l(k)N_n(d)M_r(m)W_w(k_{sp}) \tag{60a}$$

$$\mathbf{A}^*_\rho = \mathbf{A}_{ijlnrw} = \begin{bmatrix} 0 & 1 & 0 & 0 & 0 \\ \frac{-k_l}{m_r} & \frac{-d_n}{m_r} & \frac{A}{m_r} & 0 & 0 \\ 0 & -Ah_j & 0 & h_j g_i & 0 \\ 0 & 0 & 0 & 0 & 1 \\ 0 & 0 & 0 & -\omega_v^2 & -2\xi_v\omega_v \end{bmatrix} \tag{60b}$$

$$\mathbf{B}^*_\rho = \mathbf{B}_{ijlnrw} = \begin{bmatrix} 0 & 0 & 0 & 0 & k_{sp_w}\omega_v^2 \end{bmatrix}^T \tag{60c}$$

Note that $S_l(k)$, $N_n(d)$, $M_r(m)$ and $W_w(k_{sp})$ are the membership functions related to the stiffness k, total damping d, total mass m, and valve gain k_{sp}, respectively, and $\rho = w+2(r-1)+4(n-1)+8(l-1)+16(j-1)+32(i-1)$. Uncertainties related to the bulk modulus β and the supply pressure P_s are considered through calculations of g_i and h_j, (see Eqs. 14–22). For $P_L \in [\ -(2/3)P_s \quad (2/3)P_s\ ]$, which $P_s \in [\ 13.8 \quad 18.6\ ]$ MPa, $x_p \in [\ -0.05m \quad 0.05m\ ]$, and starting from the middle-point ($V_{01} = V_{02} = V_t/2$), the extremums of g_i and h_j are calculated as follows:

$$\begin{aligned} g_1 &= \max(z_1(t)) = \max\left(\frac{K_v w}{\sqrt{2}}\sqrt{P_s - \mathrm{sgn}(x_v)P_L}\right) \\ &= \frac{K_v w}{\sqrt{2}}\sqrt{18.6\text{ MPa} + \left(\frac{2}{3}\times 18.6\right)\text{ MPa}} = 2.287\text{ m}^5\text{Pa/kg}^3 \end{aligned} \tag{61a}$$

$$\begin{aligned} g_2 &= \max(z_1(t)) = \min\left(\frac{K_v w}{\sqrt{2}}\sqrt{P_s - \mathrm{sgn}(x_v)P_L}\right) \\ &= \frac{K_v w}{\sqrt{2}}\sqrt{13.6\text{ MPa} - \left(\frac{2}{3}\times 13.6\right)\text{ MPa}} = 0.881\text{ m}^5\text{Pa/kg}^3 \end{aligned} \tag{61b}$$

$$\begin{aligned} h_1 &= \max(z_2(t)) = \max\left(\frac{\beta}{0.5V_t + Ax_p} + \frac{\beta}{0.5V_t - Ax_p}\right) \\ &= \left(\frac{\beta}{0.5V_t + A(0.05)} + \frac{\beta}{0.5V_t - A(0.05)}\right) = 5.233\times 10^{12}\text{ Pa/m}^3 \end{aligned} \tag{61c}$$

$$\begin{aligned} h_2 &= \min(z_2(t)) = \min\left(\frac{\beta}{0.5V_t + Ax_p} + \frac{\beta}{0.5V_t - Ax_p}\right) \\ &= \left(\frac{\beta}{0.5V_t + A(0.0)} + \frac{\beta}{0.5V_t - A(0.0)}\right) = 5.163\times 10^{12}\text{ Pa/m}^3 \end{aligned} \tag{61d}$$

The equations describing T–S fuzzy model of the hydraulic actuator can easily blend with the equations describing the linear QFT controller. Therefore, to present the T–S fuzzy model of the closed-loop system, the state-space model of the QFT controller (54), is added to the T–S fuzzy model of the hydraulic actuator in Eqs. (59):

$$\dot{\vec{\mathbf{x}}}(t) = \sum_{\rho=1}^{64}\left(q_\rho\left(z(t)\right)\right)\left(\mathbf{A}^*_\rho\vec{\mathbf{x}}(t) + \mathbf{B}^*_\rho\mathbf{C}_c\vec{\mathbf{x}}_c\right) \tag{62a}$$

$$\dot{\vec{\mathbf{x}}}_c = \mathbf{A}_c\vec{\mathbf{x}}_c + \mathbf{B}_c(x_{p\,\text{desired}} - x_p) \tag{62b}$$

Since $\sum_{\rho=1}^{64} q_\rho\left(z(t)\right)=1$, the above equations are combined as follows:

$$\begin{bmatrix} \dot{\vec{\mathbf{x}}} \\ \dot{\vec{\mathbf{x}}}_c \end{bmatrix} = \sum_{\rho=1}^{64} q_\rho(z(t)) \left(\begin{pmatrix} \mathbf{A}_\rho^* & \mathbf{B}_\rho^* \mathbf{C}_c \\ -\mathbf{B}_c[1 \quad (0)_{1\times 4}] & \mathbf{A}_c \end{pmatrix} \begin{bmatrix} \vec{\mathbf{x}} \\ \vec{\mathbf{x}}_c \end{bmatrix} + \begin{bmatrix} (0)_{5\times 1} \\ \mathbf{B}_c \end{bmatrix} x_{p\,\text{desired}} \right) \tag{63}$$

Equation (63) describes the T–S fuzzy model of the QFT positioning control system shown in Fig. 3. To investigate the nonlinear stability of this control system first we set $\dot{\vec{\mathbf{x}}} = [\dot{x}_p \;\; \dot{v}_p \;\; \dot{P}_L \;\; \dot{x}_v \;\; \dot{v}_v \;\; \dot{x}_{c1} \;\; \cdots \;\; \dot{x}_{c\lambda}]^{\mathrm{T}} = 0$, to obtain the equilibrium point as follows:

$$\vec{\mathbf{x}}_{eq} = \begin{bmatrix} x_{p\,\text{desired}} & 0 & \frac{k x_{p\,\text{desired}}}{A} & 0 & 0 & x_{ceq1} & \ldots & x_{ceq\lambda} \end{bmatrix}^{\mathrm{T}} \tag{64}$$

This equilibrium point is not at the origin; therefore we define $\vec{\mathbf{e}} = \vec{\mathbf{x}} - \vec{\mathbf{x}}_{eq}$ and derive the following error dynamic equations:

$$\begin{bmatrix} \dot{\vec{\mathbf{e}}} \\ \dot{\vec{\mathbf{e}}}_c \end{bmatrix} = \sum_{\rho=1}^{64} q_\rho(z(t)) \underbrace{\begin{pmatrix} \mathbf{A}_\rho^* & \mathbf{B}_\rho^* \mathbf{C}_c \\ -\mathbf{B}_c[1 \quad (0)_{1\times 4}] & \mathbf{A}_c \end{pmatrix}}_{A_{\text{closed-loop}}} \begin{bmatrix} \vec{\mathbf{e}} \\ \vec{\mathbf{e}}_c \end{bmatrix} \tag{65}$$

where $\mathbf{A}_{\text{closed-loop}}$ is as follows:

$$\mathbf{A}_{\text{closed-loop}} = \begin{bmatrix} 0 & 1 & 0 & 0 & 0 & [0]_{1\times\lambda} \\ \frac{-k_l}{m_r} & \frac{-d_n}{m_r} & \frac{A}{m_r} & 0 & 0 & [0]_{1\times\lambda} \\ 0 & -Ah_j & 0 & h_j g_i & 0 & [0]_{1\times\lambda} \\ 0 & 0 & 0 & 0 & 1 & [0]_{1\times\lambda} \\ 0 & 0 & 0 & -\omega_v^2 & -2\xi_v\omega_v & k_{sp_w}\omega_v^2[\mathbf{C}_c]_{1\times\lambda} \\ [-\mathbf{B}_c]_{\lambda\times 1} & [0]_{\lambda\times 1} & [0]_{\lambda\times 1} & [0]_{\lambda\times 1} & [0]_{\lambda\times 1} & [\mathbf{A}_c]_{\lambda\times\lambda} \end{bmatrix} \tag{66}$$

Note that for the QFT controller in Eq. (53), with the state-space representation in Eqs. (54–55), λ=3. The stability of the system described by Eqs. (65–66), can now be investigated by T–S fuzzy stability theorem. Based on the stability conditions in (32), the corresponding LMIs are constructed. It was found that in order to find feasible LMIs, the uncertainty ranges for some of the parameters presented in Table 3, must be reduced. Given the new range of uncertain parameters, the following positive definite matrix $\mathbf{P}$ is obtained:

$$P = \begin{bmatrix} 2.78 & -6.5 & 441.4 & 1283 & 1387 & 624 & 963 & -15.4 \\ -6.5 & 198 & -5.4 & -232 & -74.5 & -30 & -47 & -52 \\ 441.4 & -5.4 & 315.7 & 228.4 & 119.4 & 106 & 151.1 & -7.4 \\ 1283 & -232 & 228.4 & 2502 & 1868 & -451.7 & 582 & -35.9 \\ 1387 & -74.5 & 119.4 & 1868 & 2361.4 & 851.3 & 1099.5 & 231.8 \\ 624 & -30 & 106 & -451.7 & 851.3 & 2141 & 1389 & 821.5 \\ 963 & -47 & 151.1 & 582 & 1099.5 & 1389 & 1927.4 & 690.8 \\ -15.4 & -52 & -7.4 & -35.9 & 231.8 & 821.5 & 690.8 & 855.4 \end{bmatrix} \tag{67}$$

Table 4 compares the ranges of parameters, for which the feasible LMIs have been obtained, with the ones used to design the QFT position controller. Accordingly, the nonlinear stability of the QFT controller, designed for the parametrically uncertain hydraulic actuator was proven using T–S fuzzy modeling and its stability theorem.

Table 4. Uncertainty ranges used in QFT design and proven stable by T–S fuzzy modeling approach.

Parameter	Range used in QFT design	Range for feasible LMIs
Supply pressure, P_s (MPa)	13.8–18.6	13.8–18.6
Load mass, m (kg)	11–13.7	11–11.4
Total damping, d (N·sec/m)	200–300	200–300
Fluid bulk modulus, β (MPa)	345–1030	690–710
Spool position gain, k_{sp} (μm/V)	25–31	25.1–30.7
Load stiffness, k (kN/m)	0–60	20–36

4. CONCLUSIONS

This paper investigated the nonlinear stability of QFT controllers designed for hydraulic actuators. It was shown how hydraulic functions, in a valve-controlled system having parametric uncertainties, are described as weighted sum of linear Takagi–Sugeno (T–S) fuzzy models, and blended with QFT controllers. The stability conditions of the entire system were then established via linear matrix inequalities. In order to validate the functionality of the approach, the stability of two well-established controllers for hydraulic actuators was re-examined. The first system was a nonlinear pressure controller developed for a hydraulic actuator based on the passivity theory. Using the proposed approach, the stability results were consistent with those obtained from the passivity theory. This case study validated the formulation of our model and programming. The second system was a bilateral haptic controller for a hydraulic actuator designed based on Lyapunov theory. For this control system, the proposed approach was able to not only establish the existing stability results, but also further extend the stability region to include parametric uncertainties. Having successful results from the validation case studies, the stability of a QFT position controller was analyzed for the first time. Prior to this work, the stability of this QFT controller was only shown for a defined set of inputs-outputs and in a small-signal sense. T–S fuzzy model and its stability approach provided the opportunity to prove the nonlinear stability of the QFT controller in the presence of parametric uncertainties. The results of this work, which is believed to be a further contribution to development of advanced tools for controller synthesis in fluid power actuation, clearly showed the effectiveness of using T–S models of combined hydraulics and QFT controllers, for stability verification. To summarize, in this paper we showed how to effectively solve the nonlinear stability problem of QFT controllers applied to hydraulic systems with parametric uncertainties. Using T–S fuzzy modeling and its stability theorem, the stability analysis is carried out after the controller is designed. Therefore, unnecessary and conservative conditions during the controller design are avoided. The methodology also facilitates the separation process of controller design and stability analysis of fluid power as well as other nonlinear systems.

ACKNOWLEDGEMENTS

The authors would like to thank Natural Sciences and Engineering Research Council (NSERC) of Canada and the University of Manitoba for providing financial support for this research.

REFERENCES

1. Merritt, H., *Hydraulic Control Systems*, John Wiley & Sons, 1967.
2. Melik-Gaikazov, V.I., Navrotskii, K.L. and Romashkin, M.B. “Control systems of hydraulic drives of crane mechanisms”, *Russian Engineering Journal*, Vol. 55, No. 10, pp. 56–60, 1975.
3. Fleischfresser, W., “Hydraulic systems in mobile aerial work platforms”, *Diesel Progress, International Edition*, Vol. 22, No. 4, pp. 42–44, 2003.
4. Zhang, K., Huang, X., Chen, J. and Wang, J., “GTWZ-6012 type aerial work platform hydraulic legs of stress analysis and calculation”, *Advanced Materials Research*, Vols. 308–310, pp. 2527–2530, 2011.

5. Hrovat, D., "Survey of advanced suspension developments and related optimal control applications", *Automatica*, Vol. 33, No. 10, pp. 1781–1817, 1997.
6. Zhu, W.H. and Piedboeuf, J.C., "Adaptive output force tracking control of hydraulic cylinders with application to robot manipulators", *ASME Journal of Dynamic Systems, Measurement, and Control*, Vol. 127, No. 2, pp. 206–217, 2005.
7. Bobrow, J.E. and Lum, K., "Adaptive, high bandwidth control of a hydraulic actuator", *ASME Journal of Dynamic Systems, Measurement, and Control*, Vol. 118, No. 4, pp. 714–20, 1996.
8. Guan, C. and Pan, S., "Adaptive sliding mode control of electro-hydraulic system with nonlinear unknown parameters", *Control Engineering Practice*, Vol. 16, pp. 1275–1284, 2008.
9. Liu, R. and Alleyne, A., "Nonlinear force/pressure tracking of an electro-hydraulic actuator", *ASME Journal of Dynamic Systems, Measurement, and Control*, Vol. 122, No. 1, pp. 232–237, 2000.
10. Kim, H.M., Park, S.H., Song, J.H. and Kim, J.S., "Robust position control of electro-hydraulic actuator systems using the adaptive back-stepping control scheme", *Proceedings of the Institution of Mechanical Engineers, Part I: Journal of Systems and Control Engineering*, Vol. 224, No. 6, pp. 737–746, 2010.
11. Liu, G.P. and Daley, S., "Optimal-tuning PID controller design in the frequency domain with application to a rotary hydraulic system", *Control Engineering Practice*, Vol. 7, No. 7, pp. 821–30, 1999.
12. Laval, L., M'Sirdi, N.K. and Cadiou, J.C., "H_8-force control of a hydraulic servo-actuator with environmental uncertainties", *Proceedings of IEEE International Conference on Robotics and Automation*, Vol. 2, pp. 1566–1571, 1996.
13. Niksefat, N. and Sepehri, N., "Designing robust force control of hydraulic actuators despite system and environmental uncertainties", *IEEE Control Systems Magazine*, Vol. 21, No. 2, pp. 66–77, 2001.
14. Karpenko, M. and Sepehri, N., "Equivalent time-invariant modelling of electrohydraulic actuators with application to robust control synthesis", *International Journal of Fluid Power*, Vol. 9, No. 3, pp. 7–18, 2008.
15. Raptis, I.A. and Valavanis, K.P., *Linear and Nonlinear Control of Small-Scale Unmanned Helicopters*, Springer, 2011.
16. Alleyne, A. and Liu, R., "Systematic control of a class of nonlinear systems with application to electrohydraulic cylinder pressure control", *IEEE Transactions on Control System Engineering*, Vol. 8, No. 4, pp. 623–634, 2000.
17. Karpenko, M. and Sepehri, N., "Hardware-in-the-loop simulator for research on fault tolerant control of electrohydraulic actuators in a flight control application", *Mechatronics*, Vol. 19, No. 7, pp. 1067–1077, 2009.
18. Karpenko, M. and Sepehri, N., "Electrohydraulic force control design of a hardware-in-the-loop load emulator using a nonlinear QFT technique", *Control Engineering Practice*, Vol. 20, No. 6, pp. 598–609, 2012.
19. Esfandiari, M. and Sepehri, N., "On high bandwidth output pressure control design of hydraulic actuators using quantitative feedback theory", *Transactions of the CSME*, Vol. 38, No. 4, pp. 533–555, 2014.
20. Kim, J., Xuan, D. and Kim, Y., "Robust control application for a three-axis road simulator", *Journal of Mechanical Science and Technology*, Vol. 25, No. 1, pp. 221–231, 2011.
21. Horowitz, I.M., "Synthesis of feedback systems with nonlinear time-varying uncertain plants to satisfy quantitative performance specifications", *IEEE Transactions on Automatic Control*, Vol. 20, No.4, pp. 454–464, 1976.
22. Barreiro, A. and Banos, A., "Nonlinear robust stabilization by conicity and QFT techniques", *Automatica*, Vol. 36, No. 9, pp. 1309–1320, 2000.
23. Wang, T.S., Hwang, Y.C., and Tsai, T.P., "Synthesis of feedback control systems with large plant uncertainty and time-varying gain", *International Journal of Control*, Vol. 51, No.3, pp. 687–704, 1990.
24. Oldak, S., Baril, C. and Gutman, P.O., "Quantitative design of a class of nonlinear systems with parameter uncertainty", *International Journal of Robust and Nonlinear Control*, Vol. 4, pp. 101–117, 1994.
25. Banos, A., "Nonlinear quantitative feedback theory", *International Journal of Robust and Nonlinear Control*, Vol. 17, pp. 181–202, 2007.
26. Banos, A., Barreiro, A., Gordillo, F. and Aracil, J., "A QFT framework for nonlinear robust stability", *International Journal of Robust and Nonlinear Control*, *(Isaac Horowitz Special Issue)*, Vol. 12, No. 12, pp. 357–372, 2002.
27. Banos, A. and Horowitz, I. M. "Nonlinear quantitative stability", *International Journal of Robust and Nonlinear Control*, Vol. 14, pp. 289–306, 2004.

28. Tanaka, K. and Sugeno, M., "Stability analysis and design of fuzzy control systems", *Fuzzy Sets and Systems*, Vol. 45, No. 2, pp. 135–156, 1992.
29. Tanaka, K. and Wang, H., *Fuzzy Control Systems Design and Analysis*, John Wiley & Sons, 2001.
30. Du, H. and Zhang, N., "Static output feedback control for electrohydraulic active suspensions via T–S fuzzy model approach", *Journal of Dynamic Systems, Measurement and Control*, Vol. 131, No. 5, pp. 1004–1015, 2009.
31. Du, H. and Zhang, N., "Takagi–Sugeno fuzzy control scheme for electrohydraulic active suspensions", *Control and Cybernetics*, Vol. 39, No. 4, pp. 1096–1115, 2010.
32. Boyd, S., El Ghaoui, L., Feron, E. and Balakrishnan, V., *Linear Matrix Inequalities in System and Control Theory*, SIAM, 1994.
33. Gahinet, P., Nemirovski, A., Laub, A. J. and Chilali, M., *LMI Control Toolbox*. The MathWorks Inc, 1995.
34. Zarei-Nia, K. and Sepehri, N., "Lyapunov stable displacement-mode haptic manipulation of hydraulic actuators: Theory and experiment", *International Journal Control*, Vol. 85, No. 9, pp. 1313–1326, 2012.
35. Nakkarat, P., and Kuntanapreeda, S., "Observer-based backstepping force control of an electrohydraulic actuator", *Control Engineering Practice*, Vol. 17, No. 8, pp. 895–902, 2009.
36. Wang, X., Sun, X., Li, S. and Ye, H., "Output feedback domination approach for finite-time force control of an electrohydraulic actuator", *IET control theory & applications*, Vol. 6, No.7, pp. 921–934, 2012.
37. Schmidt, T., "Adaptive backstepping control of asymmetric electro-hydraulic actuator system", Master Thesis, Aalborg University, 2012.